Revealing the Nature of Photoluminescence Emission in the Metal-Halide Double Perovskite Cs$_2$AgBiBr$_6$

S. J. Zelewski,[†,‡] J. M. Urban,[†] A. Surrente,[†] D. K. Maude,[†] A. Kuc,[¶] L. Schade,[§] R. D. Johnson,[§] M. Dollmann,[§] P. K. Nayak,[§] H. J. Snaith,[§] P. Radaelli,[§] R. Kudrawiec,[‡] R. J. Nicholas,[§] P. Plochocka,[*,†] and M. Baranowski[*,†,‡]

[†]*Laboratoire National des Champs Magnétiques Intenses, UPR 3228, CNRS-UGA-UPS-INSA, Grenoble and Toulouse, France*
[‡]*Department of Experimental Physics, Faculty of Fundamental Problems of Technology, Wroclaw University of Science and Technology, Wroclaw, Poland*
[¶]*Helmholtz-Zentrum Dresden-Rossendorf, Abteilung Ressourcenökologie, Forschungsstelle Leipzig, Permoserstr. 15, 04318, Leipzig, Germany*
[§]*University of Oxford, Clarendon Laboratory, Parks Road, Oxford, OX1 3PU, United Kingdom*

E-mail: paulina.plochocka@lncmi.cnrs.fr; michal.baranowski@lncmi.cnrs.fr

June 14, 2019

phonon interaction in this material.

Abstract

Double perovskite crystals such as Cs$_2$AgBiBr$_6$ are expected to overcome the limitation of classic hybrid organic-inorganic perovskite crystals related to the presence of lead and the lack of structural stability. Perovskites are ionic crystals in which the carriers are expected to strongly couple to lattice vibrations. In this work we demonstrate that the photoluminescence (PL) emission in Cs$_2$AgBiBr$_6$ is strongly influenced by the strong electron-phonon coupling. Combining photoluminescence excitation (PLE) and Raman spectroscopy we show that the PL emission is related to a color center rather than a band-to-band transition. The broadening and the Stokes shift of the PL emission from Cs$_2$AgBiBr$_6$ is well explained using a Franck-Condon model with a Huang-Rhys factor of $S = 11.7$ indicating a strong electron-

Introduction

Lead-halide perovskite crystals have emerged as promising materials for photovoltaic applications. After less than a decade of development perovskite solar cells already exceed 20% power conversion efficiency,[1–3] with the latest records above 23%,[3] establishing solution-processable technology as a viable alternative or extension to silicon solar cells.[4,5] This tremendous progress in perovskite-based photovoltaics is related to the unique combination of large optical absorption coefficient, long carrier lifetime and diffusion length, and low effective masses of carriers in these materials.[6–10] With their simple and cheap fabrication technology the lead-halide perovskites seems to be ideal candidates for photovoltaic and other light emitting applications.[11–13]

Despite their superior properties, the lead-

1

halide perovskites have drawbacks which hinder the deployment of this technology on a large scale. Lead-halide perovskites tend to degrade when exposed to moisture, heat, or prolonged illumination in air.[14] Even in the most stable compounds the practical lifetime of solar cells is limited to weeks rather than years.[15] In addition, the presence of Pb in solar cells is environmentally undesirable, with the formation of PbI_2 during the degradation of perovskites.[16,17]

It is expected that the intrinsic limitations of lead-halide perovskites can be overcome by the heterovalent substitution of Pb^{2+} by pairs of cations with formal oxidation states +1 and +3 forming so-called "double perovskite" with general formula $A_2^I B^I B^{III} X_6$.[17–20] Here A is a cation, for example Cs^+, filling space between halide (X= Cl, Br, I) octahedral cages. The +1 and +3 cations alternate along the x, y and z axes in neighbouring halide cages. There are numerous combinations of 1+ and 3+ ions with a suitable electron configuration such as Cu^+, Ag^+, Bi^{3+}, Sb^{3+}, and In^{3+}. Band structure calculations show that many of these compounds have a band gap in the range promising for solar cell applications.[21] Some of the possible compounds have already been synthesized corroborating theoretical predictions.[22–26] For example silver-bismuth double perovskites are highly stable[21,24] indirect band gap semiconductors with the absorption edge in the range of 1.8-2.2 eV $(Cs_2AgBiBr_6)$[24,25,27] and 2.2-2.8 eV $(Cs_2AgBiCl_6)$.[21,24,25] Moreover, recent studies have shown that these materials are very well situated for the detection of high energy radiation[28,29] and white light emitters.[30]

Metal halide perovskites are ionic crystals built from closed-shell rare-gas-like ions so that a strong interaction of the carriers with the lattice vibrations is expected.[31–33] The importance of electron-phonon coupling has already been demonstrated for a variety of perovskite semiconductors.[10,34–40] However, for double perovskites most studies have focused on structural, band gap and stability properties. The electron-phonon coupling has only received attention very recently[30,35,40,41] even though this interaction is crucial for understanding the electrical and optical properties of perovskite crystals.

In this work we show that the photoluminescence (PL) emission in $Cs_2AgBiBr_6$ is dominated by a strong electron-phonon interaction. Using a combination of PL, Raman and photoluminescence excitation (PLE) we reveal that the PL emission is related to a color center rather than a band-to-band transition. The resonant excitation of this center results in a strong enhancement of PL emission demonstrating the importance of the non-radiative recombination path related to the indirect bandgap. Crucially, we show that the significant PL broadening together with the large Stokes shift between emission (PL) and absorption (PLE) can be well explained using a configurational coordinate diagram (Franck-Condon model) indicating a strong electron-phonon coupling characterized by a relatively large Huang-Rhys factor $\simeq 12$.

Methods

Experiment

The investigated sample was a $\simeq 1 \times 1 \times 1$ mm^3 single crystal obtained from the dissolved poly-crystalline powder ($\simeq 1$g) in $\simeq 10$ mL of 9-M HBr. The solution was cooled down from $110\,°C$ at a rate of $0.5\,°C$/hour. An extended description of the crystal synthesis and structural characterization can be found in ref.[42]

Sample were mounted in a helium cryostat. Optical access to the samples was provided through a quartz window. The PL, Raman spectra and PLE measurements were performed in the backscattering configuration. PL and PLE was excited provided by femtosecond pulse (150 fs) mode-locked Ti:sapphire laser or frequency doubled output of an optical parametric oscillator, synchronously pumped by the Ti:sapphire laser. The excitation beam was focused on the sample by a 20 cm focal length lens. The emitted PL was collected through the same lens and redirected to a spectrometer equipped with a liquid nitrogen cooled charge-coupled device camera. The reflectivity spectrum was measured exciting with a tungsten
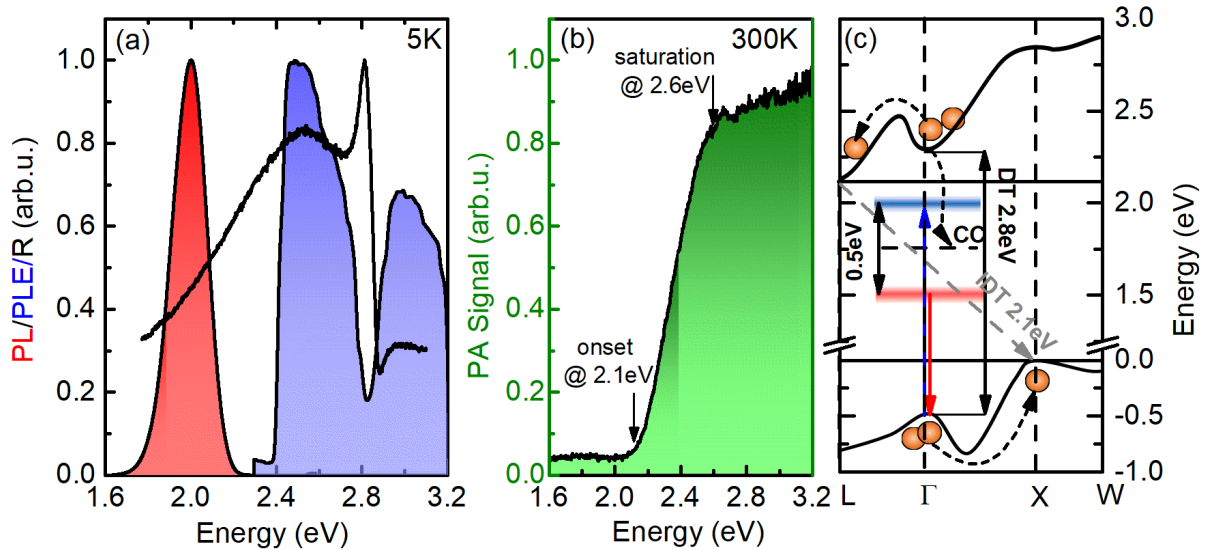
Figure 1: (a) Low temperature ($T = 5\,\mathrm{K}$) photoluminescence spectrum (PL in red) and integrated PL intensity as a function of the energy of the exciting photons (PLE spectrum in blue) together with the reflectance spectrum (R in black). (b) photoacoustic signal (PAS) as a function of the excitation energy (equivalent to absorption) measured at $300\,\mathrm{K}$. (c) Schematic showing the band structure of ($Cs_2AgBiBr_6$) with possible transitions and carrier relaxation pathways. The black dashed line indicates the position of color centers. The blue and red bars represent absorption and emission bands of the color center which are broadened and shifted from the energy of equilibrium state of color center (dashed line) due to the strong electron-phonon coupling (see text).

halogen lamp. Raman scattering measurements were performed at $T = 5\,\mathrm{K}$ with the use of cw $532\,\mathrm{nm}$ laser. The laser beam power was $0.2\,\mathrm{mW}$. The excitation beam was focused on the sample by a ×50 microscope objective with a numerical aperture of 0.55. Photoacoustic spectra were measured in the microphone sensing configuration. A tunable light source consisting of a 250 W tungsten halogen lamp and a 0.32 m focal length monochromator was used to illuminate the sample mounted inside a non-resonant photoacoustic cell. The incident beam was modulated with a mechanical chopper at a frequency of 40 Hz, passed through a quartz transmission window, and focused to a spot of 2 mm x 1 mm in size. Acoustic waves arising inside the air-tight cell were detected with an electret condenser microphone producing a voltage signal further demodulated with a lock-in amplifier (Stanford Research Systems SR830).

Theory

All calculations were performed using DFT as implemented in the Crystal17 code.[43,44] The system was fully relaxed (atomic positions and lattice vectors) using PBE functional[45] with van der Waals correction as proposed by Grimme[46] and the effective core potential basis sets to account for relativistic effects. Optimization was performed using 36 k-point mesh in the irreducible Brillouin zone following the Monkhorst-Pack approach. Raman spectra were calculated from the dielectric tensor with the Coupled Perturbed Hartree-Fock (CPHF) method, as implemented in Crystal17 code. Two models were used to represent the $Cs_2AgBiBr_6$ crystal structure, the cubic form ($Fm\bar{3}m$, #225) and the tetragonal form ($I4/m$, #87) in order to understand the changes in Raman shifts with respect to the lattice vectors.

Results and Discussion

Figure 1 (a) shows the PL (red), PLE (blue) and reflectance (black line) spectra of $Cs_2AgBiBr_6$ single crystal taken at $T = 5\,K$. The PL emission, centered around $2\,eV$ is strongly broadened, with a full width half maximum (FWHM) of $\simeq 190\,meV$. The PLE spectrum shows that the intensity of the PL emission strongly depends on the energy of the exciting photons. For excitation below $2.4\,eV$ the PL emission is almost completely quenched. For excitation above $2.4\,eV$ the PL signal increases rapidly reaching a maximum at around $2.5\,eV$ before decreasing slowly at higher energies. A sharp decrease of PLE signal is observed around $2.8\,eV$ corresponding to the direct band gap exciton which is clearly visible as a resonance in the reflectance spectrum (see black lines in Fig. 1 (a)).[42] This behaviour is unusual for band-to-band transitions where the PLE signal normally shows a monotonic increase[47] simply following the increasing density of states of the bands before eventually saturating for strong enough absorption. The complex dependence of PLE signal is in contrast to photoacoustic (PA) spectrum (equivalent to absorption) presented in Fig.1 (b). The photoacoustic signal onset is around $2.1\,eV$ (Tauc plot analysis presented in supporting information gives a bandgap energy of $2.12\,eV$) and monotonic increase can be observed before saturation of PA signal at around $2.6\,eV$. Similarly reported absorption spectra exhibit monotonic increase from around $2.1\,eV$ up to direct bandgap transition around $2.8\,eV$[18,27,48,49] (see also fig. S1 in supporting information). Moreover the onset of PLE is at hundreds of meV higher than the reported bandgap for $Cs_2AgBiBr_6$.[24,25,27,48]

The non-monotonic behaviour of the PLE signal indicates that the observed PL emission is not related to a band-to-band transition, but its origin can be attributed to a color center, which can be effectively (directly) excited by $2.5\,eV$ photons. The density of color centers and their photon absorption cross-section cannot be very high, since they are not seen in the absorption spectrum. Excitation above or below $2.5\,eV$ energy results in a quenching of the PL signal since the emitting states are no longer populated/excited effectively. This can be understood as a competition between recombination pathways; in the case of off-resonant excitation, photocreated carriers can either be trapped by the color centers or they can relax to the minimum of the indirect band gap, as shown schematically in Fig. 1(c). The significant drop of PL signal for excitation different than $2.5\,eV$ suggests that the carriers created in the band states mostly relax to the minimum of the bands corresponding to indirect band gap where they recombine non-radiatively. Further evidence of competition between band states and emissive color-center states can be seen from the sharp dip in the PLE spectrum at $2.8\,eV$, which correspond to the direct-gap excitonic absorption. Despite expected significant increase in absorption for excitonic transition at $2.8\,eV$ (visible in reflectance and absorption spectrum presented in SI), the PL signal decreases. One of the possible explanations might be related to the neutral character of the exciton, which inhibits trapping by the color-center/trap states. The excitons are formed directly only in the case of resonant excitation at $2.8\,eV$, while the higher energy excitation results in the creation of free electrons and holes, a small fraction of which, can relax to the color-center states, before they have time to form excitons or relax to the band minima, which might explain increase of the PLE signal above $2.8\,eV$. This scenario of carrier relaxation and recombination is in agreement with the recent studies of PL and transient absorption dynamics, which show that majority of the carriers relax to the indirect band gap states and later recombine non-radiatively.[49,50]

In ionic crystals color centers are usually strongly coupled to the crystal lattice vibrations.[31] The occupation of such a center causes a local lattice deformation leading to an energy offset between the ground (unoccupied) and excited (occupied) states of the color center. Radiative recombination can then occur accompanied by the emission of multiple phonons.[31,51] This leads to a broadening of the absorption and emission bands, which are energetically separated as shown schematically in Fig. 1 (c).
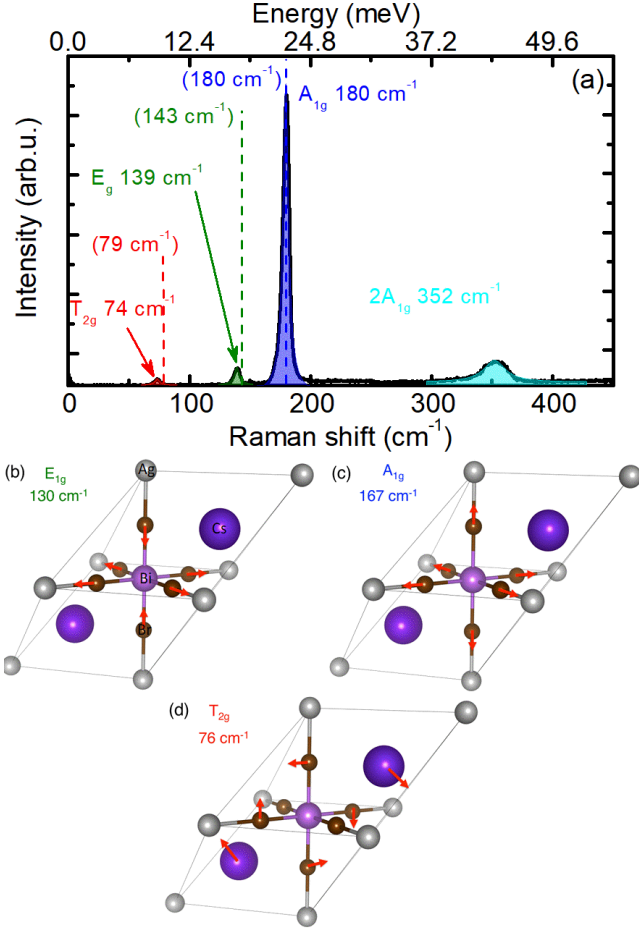
Figure 2: Low temperature (5 K) Raman spectrum of $Cs_2AgBiBr_6$. The experimental peaks are represented by solid lines while the Lorentzian fits are represented by shaded area. The dashed lines indicate the energy of vibration calculated using DFT. (b)-(d) schema of the lattice vibration visible in Raman spectrum.

The observed $\simeq 500$ meV Stokes shift between emission (PL) and absorption (PLE) together with the significant broadening of the PL emission are the smoking gun signature of a strong electron-phonon coupling in $Cs_2AgBiBr_6$.

The strength of the electron-phonon interaction is characterized by the Huang-Rhys factor S which is the average number of phonons emitted by the color center after photon absorption or emission. The phonon energy can be extracted from the Raman spectrum presented in Fig. 2. The low temperate Raman spectrum is dominated by the peak at 180 cm^{-1} and two less intense peaks can be seen at 139 cm^{-1} and 74 cm^{-1}. We identify the origin of each

peak comparing it with the predictions of DFT calculations (see supplementary information for DFT details) marked by the vertical dashed lines. The peak around 180 cm^{-1} is the A_{1g} LO phonon mode related to symmetric stretching vibration of Br atoms around Bi atoms in the octahedron and the two lower peaks are vibration with symmetries of E_g (at around 139 cm^{-1}) and T_{2g} (at around 74 cm^{-1}). The E_g mode is related to the asymmetric stretching vibrations of Br around Bi atoms. The T_{2g} mode is a correlated motion of Cs atoms with the scissoring of Br atoms (see . Fig. 2).

The calculated energies of the modes are slightly lower than measured experimentally, which might be related to disorder in Ag and Bi cation arrangement or a non fully relaxed crystal structure (the ionic radius of Ag is larger than that of Bi, therefore bonding distortions arise due to the large mismatch of the two sublattices[35]). The dependence of simulated Raman peaks on the lattice vectors is shown in Supporting Information (Fig. S4). The weak peak visible at around 350 cm^{-1} is usually attributed to the second order of the A_{1g} mode,[35] not observed in the DFT simulations.

According to a conventional Franck-Condon model the absorption and emission spectrum are composed of a series of transitions separated by the phonon energy E_{ph}. The intensity of each transition is proportional to the overlap of the harmonic oscillator states in the ground and excited states of the color center (see Fig.3). At low temperature only the ground vibrational state is occupied and the intensity of each transition is proportional to:

$$I(n) \sim \frac{e^{-S}S^n}{n!}. \qquad (1)$$

This predicts that the emission is a mirror image of the absorption spectrum. As the Huang-Rhys S factor the absorption and emission spectrum change from being dominated by the 0 phonon line to multiple phonon excitation and emission. This is shown in Fig. 3 (b)-(d) where we calculate the emission and absorption for different values of S and line widths of the individual phonon transitions (FWHM of
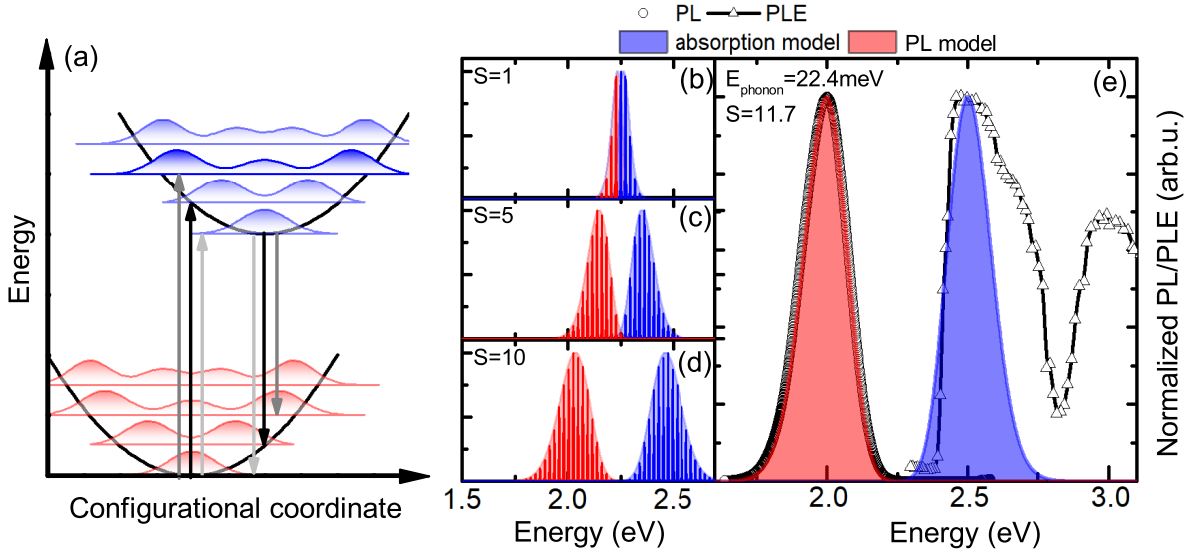
Figure 3: (a) Schematic showing the Franck-Condon model (configurational coordinate diagram). Red and blue parabole represent the harmonic potential felt by the color center in the ground and excited states. The shaded area represents spatial probability distribution of the harmonic oscillator eigen states. The arrows show transitions with 0 (light gray) 1 (black) and 2 (dark gray) phonons involved. (b) – (d) evolution of the absorption (blue) and emission spectra (red) as a function of the Huang-Rhys factor. The solid lines are spectra modelled with $1\,meV$ FWHM of each phonon assisted transition while the lighter colored shaded areas are calculated with $10\,meV$ FWHM. (e) Results of the Franck-Condon model fitting (shaded area) to the PL and PLE spectra. We assume 10 meV broadening of each phonon transition and $22.4\,meV$ phonon energy.

$1\,meV$ (blue-red) and $10\,meV$ (lighter colored shaded area)). Typically, for strong electron-phonon coupling the broadening of the phonon-assisted transitions results in smooth broad emission and absorption bands without any phonon structure.[31] The size of the Stokes shift is also controlled by the value of S, and for smooth bands (individual transitions not resolved) its value is somewhere between $(2S-1)E_{ph}$ and $2SE_{ph}$.[51] In perovskite crystals the carrier scattering is dominated by longitudinal optical (LO) phonons[35] which correspond to an energy of $\sim 22.4\,meV$ ($180\,cm^{-1}$ in the Raman spectrum) for the $Cs_2AgBiBr_6$. Assuming $E_{ph} = 22.4\,meV$ the PL and dominant PLE onset are very well reproduced using a Huang-Rhys factor of $S = 11.7$ (see Fig.3) and a 0-phonon line energy of 2.25 eV. Crucially, the Huang-Rhys factor S is the only fitting parameter and reproduces exactly the Stokes shift and the broadening of the PL lending strong support to the coupled color center model. Obviously the PLE spectrum is not reproduced with

such a good agreement as PL since it is affected by the transfer of free carriers (excited in band-to-band transitions) to color centers, nevertheless the dominant feature is well reproduced.

The exact nature of the color centre remains an open question. It can be either intrinsic, related to the self trapping of carriers or excitons, alternatively it may be trap or defect related,[31,40,52,53] any of which can strongly deform the lattice after carrier trapping. The defects themselves can be intrinsic through the presence of defects such as Ag vacancies or AgBi anti-site defects which are calculated to act as shallow acceptors[54] causing $Cs_2AgBiBr_6$ single crystals to become p-type, as has been concluded from photoemission measurements.[49] Very recently it was shown that in the case of $Cs_2AgInCl_6$ a strong PL emission is related to intrinsic hole self trapping at the Ag atom, however in the case of $Cs_2AgBiBr_6$ it has been suggested that the behaviour is defect related.[49,50] Our measurements suggest that defects may be a more likely explanation. The sig-

nificant difference between the absorption and the PLE spectra, in particular the very sharp onset at 2.4 eV, suggests that direct excitation to the emissive state is occurring consistently with a Frank-Condon model with strong carrier trapping. By contrast the significantly different absorption spectrum is thought to be dominated by the indirect band gap leading to competition between radiative and non-radiative processes. Further evidence of this can be seen from the sharp dip in the PLE spectrum at 2.8 eV which arises due to competition with the direct gap exciton which does not give rise to any color centre emission but corresponds to the dispersive feature in the reflectivity shown in Fig. 1.[42] The marked difference of the PLE signal compared to the absorption spectrum favors an extrinsic origin of the color center, as we would expect that carrier self-trapping will occur regardless of the photo-excitation energy, and after thermalization, the photo-created carriers will undergo self-localization. The defect related origin is also in agreement with recent studies of carrier dynamics[41,49,50] which suggest that PL is mediated through defect states.

It is worth noting that the $Cs_2AgInCl_6$[30] is significantly more polar than $Cs_2AgInBr_6$ due to the larger electronegativity differences between the Ag/In and Cl atoms (Cl−Ag=1.23, Cl−In=1.38) compared to Ag/Bi and Br (Br−Ag =1.03, Br−Bi=0.94) which will enhance its probability of self-trapping. This is also consistent with the significantly larger Huang-Rhys factor of 37 observed for the Chloride compared with our value of 11.7 for the Bromide.[30] A similar difference in behaviour has been reported for other metal halides such as $AgBr_{1-x}Cl_x$, where a swap over from self trapping to free excitonic behaviour has been observed as the Cl is replaced by Br.[31,32]

Conclusions

In conclusion, we have shown that the optical properties of $Cs_2AgBiBr_6$ are dominated by the strong coupling between the photoexcited carriers and phonons. The difference in the PLE and absorption spectrum demonstrates that the PL emission in this material originates from color centers rather than band-to-band recombination. The significant broadening of the PL together with the Stokes shift between PL and PLE peaks can be explained by a Franck-Condon model indicative of a strong local lattice deformation upon excitation of the color center states which is characterized by a relatively large Huang-Rhys factor of about 12. The significant variation of the PLE signal results from competitive pathways for carrier recombination, radiative recombination related to direct color center and, non-radiative recombination of the carriers which relax to the bottom of indirect band gap, combined also with direct gap excitonic absorption.

Supporting Information

Comparison of literature absorption data with PLE spectrum, Calculated phonons dispersions, Simulation of Raman spectra.

Conflicts of interest

There are no conflicts of interest to declare.

References

(1) Yang, W. S.; Park, B.-W.; Jung, E. H.; Jeon, N. J.; Kim, Y. C.; Lee, D. U.; Shin, S. S.; Seo, J.; Kim, E. K.; Noh, J. H. et al. Iodide management in formamidinium-lead-halide–based perovskite layers for efficient solar cells. *Science* **2017**, *356*, 1376–1379.

(2) Green, M. A.; Hishikawa, Y.; Dunlop, E. D.; Levi, D. H.; Hohl-Ebinger, J.; Yoshita, M.; Ho-Baillie, A. W. Solar cell efficiency tables (Version 53). *Prog. Photovoltaics* **2018**, *27*, 3–12.

(3) NREL, Best Research-Cell Efficiency Chart. https://www.nrel.gov/pv/cell-efficiency.html, Accessed 18.04.2019.

(4) Leijtens, T.; Bush, K. A.; Prasanna, R.; McGehee, M. D. Opportunities and challenges for tandem solar cells using metal halide perovskite semiconductors. *Nat. Energy* **2018**, *3*, 828–838.

(5) Sahli, F.; Werner, J.; Kamino, B. A.; BrÄuninger, M.; Monnard, R.; Paviet-Salomon, B.; Barraud, L.; Ding, L.; Leon, J. J. D.; Sacchetto, D. et al. Fully textured monolithic perovskite/silicon tandem solar cells with 25.2% power conversion efficiency. *Nat. Mater.* **2018**, *17*, 820–826.

(6) Stranks, S. D.; Eperon, G. E.; Grancini, G.; Menelaou, C.; Alcocer, M. J.; Leijtens, T.; Herz, L. M.; Petrozza, A.; Snaith, H. J. Electron-hole diffusion lengths exceeding 1 micrometer in an organometal trihalide perovskite absorber. *Science* **2013**, *342*, 341–344.

(7) de Quillettes, D. W.; Vorpahl, S. M.; Stranks, S. D.; Nagaoka, H.; Eperon, G. E.; Ziffer, M. E.; Snaith, H. J.; Ginger, D. S. Impact of microstructure on local carrier lifetime in perovskite solar cells. *Science* **2015**, *348*, 683–686.

(8) Hutter, E. M.; Gélvez-Rueda, M. C.; Osherov, A.; Bulović, V.; Grozema, F. C.; Stranks, S. D.; Savenije, T. J. Direct–indirect character of the bandgap in methylammonium lead iodide perovskite. *Nat. Mater.* **2017**, *16*, 115–120.

(9) Huang, J.; Yuan, Y.; Shao, Y.; Yan, Y. Understanding the physical properties of hybrid perovskites for photovoltaic applications. *Nat. Rev. Mater.* **2017**, *2*, 17042.

(10) Miyata, A.; Mitioglu, A.; Plochocka, P.; Portugall, O.; Wang, J. T.-W.; Stranks, S. D.; Snaith, H. J.; Nicholas, R. J. Direct measurement of the exciton binding energy and effective masses for charge carriers in organic-inorganic tri-halide perovskites. *Nat. Phys.* **2015**, *11*, 582–587.

(11) Yang, S.; Fu, W.; Zhang, Z.; Chen, H.; Li, C.-Z. Recent advances in perovskite solar cells: efficiency, stability and lead-free perovskite. *J. Mater. Chem. A* **2017**, *5*, 11462–11482.

(12) Stranks, S. D.; Snaith, H. J. Metal-halide perovskites for photovoltaic and light-emitting devices. *Nat. Nanotechnol.* **2015**, *10*, 391–402.

(13) Park, N.-G. Perovskite solar cells: an emerging photovoltaic technology. *Mater. Today (Oxford, U. K.)* **2015**, *18*, 65–72.

(14) Asghar, M.; Zhang, J.; Wang, H.; Lund, P. Device stability of perovskite solar cells–a review. *Renewable Sustainable Energy Rev.* **2017**, *77*, 131–146.

(15) Christians, J. A.; Schulz, P.; Tinkham, J. S.; Schloemer, T. H.; Harvey, S. P.; de Villers, B. J. T.; Sellinger, A.; Berry, J. J.; Luther, J. M. Tailored interfaces of unencapsulated perovskite solar cells for> 1,000 hour operational stability. *Nat. Energy* **2018**, *3*, 68–74.

(16) Flora, G.; Gupta, D.; Tiwari, A. Toxicity of lead: a review with recent updates. *Interdiscip. Toxicol.* **2012**, *5*, 47–58.

(17) Giustino, F.; Snaith, H. J. Toward lead-free perovskite solar cells. *ACS Energy Lett.* **2016**, *1*, 1233–1240.

(18) Greul, E.; Petrus, M. L.; Binek, A.; Docampo, P.; Bein, T. Highly stable, phase pure $Cs_2AgBiBr_6$ double perovskite thin films for optoelectronic applications. *J. Mater. Chem. A* **2017**, *5*, 19972–19981.

(19) Zhang, Q.; Yin, Y. All-Inorganic Metal Halide Perovskite Nanocrystals: Opportunities and Challenges. *ACS Central Science* **2018**, *4*, 668–679.

(20) Zhou, L.; Xu, Y.-F.; Chen, B.-X.; Kuang, D.-B.; Su, C.-Y. Synthesis and Photocatalytic Application of Stable Lead-Free Cs2 AgBiBr6 Perovskite Nanocrystals. *Small* **2018**, *14*, 1703762.

(21) Volonakis, G.; Filip, M. R.; Haghighirad, A. A.; Sakai, N.; Wenger, B.; Snaith, H. J.; Giustino, F. Lead-free halide double perovskites via heterovalent substitution of noble metals. *J. Phys. Chem. Lett.* **2016**, *7*, 1254–1259.

(22) Volonakis, G.; Haghighirad, A. A.; Milot, R. L.; Sio, W. H.; Filip, M. R.; Wenger, B.; Johnston, M. B.; Herz, L. M.; Snaith, H. J.; Giustino, F. Cs2InAgCl6: A new lead-free halide double perovskite with direct band gap. *J. Phys. Chem. Lett* **2017**, *8*, 772–778.

(23) Bekenstein, Y.; Dahl, J. C.; Huang, J.; Osowiecki, W. T.; Swabeck, J. K.; Chan, E. M.; Yang, P.; Alivisatos, A. P. The making and breaking of lead-free double perovskite nanocrystals of cesium silver–bismuth halide compositions. *Nano Lett.* **2018**, *18*, 3502–3508.

(24) McClure, E. T.; Ball, M. R.; Windl, W.; Woodward, P. M. Cs2AgBiX6 (X= Br, Cl): new visible light absorbing, lead-free halide perovskite semiconductors. *Chem. Mater* **2016**, *28*, 1348–1354.

(25) Filip, M. R.; Hillman, S.; Haghighirad, A. A.; Snaith, H. J.; Giustino, F. Band gaps of the lead-free halide double perovskites $Cs_2BiAgCl_6$ and $Cs_2BiAgBr_6$ from theory and experiment. *J. Phys. Chem. Lett* **2016**, *7*, 2579–2585.

(26) Du, K.-z.; Meng, W.; Wang, X.; Yan, Y.; Mitzi, D. B. Bandgap engineering of lead-free double perovskite $Cs_2AgBiBr_6$ through trivalent metal alloying. *Angew. Chem., Int. Ed.* **2017**, *56*, 8158–8162.

(27) Slavney, A. H.; Hu, T.; Lindenberg, A. M.; Karunadasa, H. I. A bismuth-halide double perovskite with long carrier recombination lifetime for photovoltaic applications. *J. Am. Chem. Soc.* **2016**, *138*, 2138–2141.

(28) Pan, W.; Wu, H.; Luo, J.; Deng, Z.; Ge, C.; Chen, C.; Jiang, X.; Yin, W.-J.; Niu, G.; Zhu, L. et al. $Cs_2AgBiBr_6$ single-crystal X-ray detectors with a low detection limit. *Nat. Photonics* **2017**, *11*, 726–732.

(29) Steele, J. A.; Pan, W.; Martin, C.; Keshavarz, M.; Debroye, E.; Yuan, H.; Banerjee, S.; Fron, E.; Jonckheere, D.; Kim, C. W. et al. Photophysical pathways in highly sensitive $Cs_2AgBiBr_6$ double-perovskite single-crystal X-ray detectors. *Adv. Mater.* **2018**, 1804450.

(30) Luo, J.; Wang, X.; Li, S.; Liu, J.; Guo, Y.; Niu, G.; Yao, L.; Fu, Y.; Gao, L.; Dong, Q. et al. Efficient and stable emission of warm-white light from lead-free halide double perovskites. *Nature* **2018**, *563*, 541–545.

(31) Pelant, I.; Valenta, J. *Luminescence spectroscopy of semiconductors*; Oxford University Press, 2012.

(32) Kanzaki, H.; Sakuragi, S.; Sakamoto, K. Excitons in AgBr1-æClæ-transition of relaxed state between free and self-traffed

exciton. *Solid State Commun.* **1971**, *9*, 999–1002.

(33) Williams, R.; Song, K. The self-trapped exciton. *J. Phys. Chem. Solids* **1990**, *51*, 679–716.

(34) Miyata, K.; Meggiolaro, D.; Trinh, M. T.; Joshi, P. P.; Mosconi, E.; Jones, S. C.; De Angelis, F.; Zhu, X.-Y. Large polarons in lead halide perovskites. *Sci. Adv.* **2017**, *3*, e1701217.

(35) Steele, J. A.; Puech, P.; Keshavarz, M.; Yang, R.; Banerjee, S.; Debroye, E.; Kim, C. W.; Yuan, H.; Heo, N. H.; Vanacken, J. et al. Giant electron-phonon coupling and deep conduction band resonance in metal halide double perovskite. *ACS nano* **2018**, *12*, 8081–8090.

(36) Cortecchia, D.; Yin, J.; Bruno, A.; Lo, S.-Z. A.; Gurzadyan, G. G.; Mhaisalkar, S.; Brédas, J.-L.; Soci, C. Polaron self-localization in white-light emitting hybrid perovskites. *J. Mater. Chem. C* **2017**, *5*, 2771–2780.

(37) Yangui, A.; Garrot, D.; Lauret, J.-S.; Lusson, A.; Bouchez, G.; Deleporte, E.; Pillet, S.; Bendeif, E.-E.; Castro, M.; Triki, S. et al. Optical investigation of broadband white-light emission in self-assembled organic–inorganic perovskite (C6H11NH3) 2PbBr4. *J. Phys. Chem. C* **2015**, *119*, 23638–23647.

(38) McCall, K. M.; Stoumpos, C. C.; Kostina, S. S.; Kanatzidis, M. G.; Wessels, B. W. Strong electron–phonon coupling and self-trapped excitons in the defect halide perovskites A3M2I9 (a= Cs, Rb; M= Bi, Sb). *Chem. Mater* **2017**, *29*, 4129–4145.

(39) Straus, D. B.; Hurtado Parra, S.; Iotov, N.; Gebhardt, J.; Rappe, A. M.; Subotnik, J. E.; Kikkawa, J. M.; Kagan, C. R. Direct observation of electron–phonon coupling and slow vibrational relaxation in organic–inorganic hybrid per-

ovskites. *J. Am. Chem. Soc.* **2016**, *138*, 13798–13801.

(40) Li, S.; Luo, J.; Liu, J.; Tang, J. Self-Trapped Excitons in All-Inorganic Halide Perovskites: Fundamentals, Status, and Potential Applications. *The Journal of Physical Chemistry Letters* **2019**, *10*, 1999–2007.

(41) Kentsch, R.; Scholz, M.; Horn, J.; Schlettwein, D.; Oum, K.; Lenzer, T. Exciton dynamics and electron-phonon coupling affect the photovoltaic performance of the $Cs_2AgBiBr_6$ double perovskite. *J. Phys. Chem. C* **2018**, *122*, 25940–25947.

(42) Schade, L.; Wright, A. D.; Johnson, R. D.; Dollmann, M.; Wenger, B.; Nayak, P. K.; Prabhakaran, D.; Herz, L. M.; Nicholas, R.; Snaith, H. J. et al. Structural and Optical Properties of Cs2AgBiBr6 Double Perovskite. *ACS Energy Lett.* **2019**, *4*, 299–305.

(43) Dovesi, R.; Erba, A.; Orlando, R.; Zicovich-Wilson, C. M.; Civalleri, B.; Maschio, L.; Rerat, M.; Casassa, S.; Baima, J.; Salustro, S. et al. Quantum-mechanical condensed matter simulations with CRYSTAL. *Wiley Interdiscip. Rev.: Comput. Mol. Sci. 8*, e1360.

(44) Dovesi, R.; Saunders, V. R.; Roetti, C.; Orlando, R.; Zicovich-Wilson, C. M.; Pascale, F.; Civalleri, B.; Doll, K.; Harrison, N. M.; Bush, I. J. et al. CRYSTAL17 User's Manual (University of Torino, Torino, 2017). CRYSTAL17 User's Manual (University of Torino, Torino, 2017).

(45) Perdew, J. P.; Burke, K.; Ernzerhof, M. *Phys. Rev. Lett.* **1996**, *77*, 3865–3868.

(46) Grimme, S. Semiempirical GGA-type density functional constructed with a long-range dispersion correction. *J. Comp. Chem.* **2006**, *27*, 1787–1799.

(47) Yang, J.; Zhang, P.; Wei, S.-H. Band structure engineering of $Cs_2AgBiBr_6$ Perovskite through Order–Disordered Tran-

sition: A First-Principle Study. *J. Phys. Chem. Lett.* **2017**, *9*, 31–35.

(48) Bartesaghi, D.; Slavney, A. H.; Gelvez-Rueda, M. C.; Connor, B. A.; Grozema, F. C.; Karunadasa, H. I.; Savenije, T. J. Charge carrier dynamics in $Cs_2AgBiBr_6$ double perovskite. *J. Phys. Chem. C* **2018**, *122*, 4809–4816.

(49) Hoye, R. L.; Eyre, L.; Wei, F.; Brivio, F.; Sadhanala, A.; Sun, S.; Li, W.; Zhang, K. H.; MacManus-Driscoll, J. L.; Bristowe, P. D. et al. Fundamental carrier lifetime exceeding 1 μs in $Cs_2AgBiBr_6$ double perovskite. *Adv. Mater. Interfaces* **2018**, 1800464.

(50) Steele, J. A.; Pan, W.; Martin, C.; Keshavarz, M.; Debroye, E.; Yuan, H.; Banerjee, S.; Fron, E.; Jonckheere, D.; Kim, C. W. et al. Photophysical pathways in highly sensitive $Cs_2AgBiBr_6$ double-perovskite single-crystal X-Ray detectors. *Adv. Mater. 30*, 1804450.

(51) de Jong, M.; Seijo, L.; Meijerink, A.; Rabouw, F. T. Resolving the ambiguity in the relation between Stokes shift and Huang–Rhys parameter. *Phys. Chem. Chem. Phys.* **2015**, *17*, 16959–16969.

(52) Smith, M. D.; Karunadasa, H. I. White-light emission from layered halide perovskites. *Acc. Chem. Res.* **2018**, *51*, 619–627.

(53) Booker, E. P.; Thomas, T. H.; Quarti, C.; Stanton, M. R.; Dashwood, C. D.; Gillett, A. J.; Richter, J. M.; Pearson, A. J.; Davis, N. J.; Sirringhaus, H. et al. Formation of long-lived color centers for broadband visible light emission in low-dimensional layered perovskites. *J. Am. Chem. Soc.* **2017**, *139*, 18632–18639.

(54) Xiao, Z.; Meng, W.; Wang, J.; Yan, Y. Thermodynamic stability and defect chemistry of bismuth-based lead-free double perovskites. *ChemSusChem* **2016**, *9*, 2628–2633.

Graphical TOC Entry
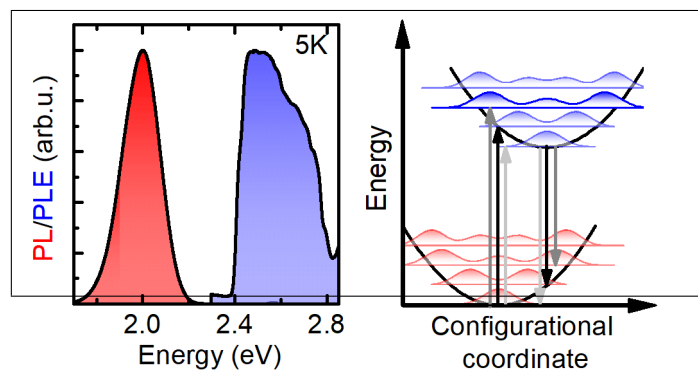
The emission and absorption of $Cs_2AgBiBr_6$ are dominated by the strong carriers-phonon coupling.